

CD9 tetraspanin generates fusion competent sites on the egg membrane for mammalian fertilization

Antoine Jégou^a, Ahmed Ziyat^{b,c}, Virginie Barraud-Lange^{a,b,c}, Eric Perez^a, Jean Philippe Wolf^{b,c}, Frédéric Pincet^a, and Christine Gourier^{a,1}

^aLaboratoire de Physique Statistique, Ecole Normale Supérieure de Paris, Université Pierre et Marie Curie, Université Paris Diderot, Centre National de la Recherche Scientifique, 24 rue Lhomond, 75005 Paris, France; ^bUniversité Paris Descartes, Institut National de la Santé et de la Recherche Médicale U1016, Génétique, Epigénétique et Physiopathologie de la Reproduction, 24 rue du Faubourg Saint-Jacques, Paris F-75014, France; and ^cService d'histologie, d'embryologie, Biologie de la Reproduction, Hôpital Cochin, Assistance Publique-Hôpitaux de Paris, Université Paris Descartes, 123, Bd Port Royal, 75014 Paris, France

Edited by Nejat Duzgunes, University of the Pacific School of Dentistry, San Francisco, CA, and accepted by the Editorial Board May 23, 2011 (received for review November 20, 2010)

CD9 tetraspanin is the only egg membrane protein known to be essential for fertilization. To investigate its role, we have measured, on a unique acrosome reacted sperm brought in contact with an egg, the adhesion probability and strength with a sensitivity of a single molecule attachment. Probing the binding events at different locations of wild-type egg we described different modes of interaction. Here, we show that more gamete adhesion events occur on Cd9 null eggs but that the strongest interaction mode disappears. We propose that sperm–egg fusion is a direct consequence of CD9 controlled sperm–egg adhesion properties. CD9 generates adhesion sites responsible for the strongest of the observed gamete interaction. These strong adhesion sites impose, during the whole interaction lifetime, a tight proximity of the gamete membranes, which is a requirement for fusion to take place. The CD9-induced adhesion sites would be the actual location where fusion occurs.

force measurement | cell–cell adhesion | membrane organization | Biomembrane Force Probe | contact lifetime

Membrane fusion occurs in many contexts: virus–cell fusion, intracellular fusion, cell–cell fusion. It takes place in two steps: attachment of two membranes and physical merging of the membranes and inner contents. Numerous questions on this complex process are still open. This is particularly true for gamete fusion during fertilization. So far, among the molecular actors of sperm–egg interaction identified at the gamete membranes (1–5), CD9 tetraspanin is the only egg protein that has been proven to be essential for fertilization of mice (6–10) and other mammal species (11–13). Indeed, deletion of *Cd9* gene results in a dramatic reduction of female fertility due to a lack of fusion of sperm with *Cd9* null eggs (7, 8, 10). The mechanism by which CD9 takes part in gamete fusion still needs to be elucidated. However, the main function attributed to tetraspanins is to organize networks of cis-partner proteins within the plasma membrane (14–19). Deletion of *Cd9* tetraspanin gene has also been reported to alter the morphology of egg microvilli (20). The relation between CD9-dependent membrane organization and fusion ability needs to be clarified. If decisive for fusion, CD9-driven membrane morphology and molecular distribution could have crucial effects on gamete adhesion first, because adhesion is the first and necessary step in any fusion process. So far, combination of zona-free eggs in vitro fertilization and binding assays has shown that the lack of fusion observed for *Cd9* null eggs was not accompanied by a loss of sperm–egg adhesion (7, 8, 10). However, this method, that only allows counting the number of sperm attached to the egg membrane after an extended period of coincubation, cannot reveal any adhesion detail due to CD9-controlled membrane organization. Revealing such specificity requires the characterization of the sperm–egg attachments at the single molecule level. We have recently developed a biophysical approach allowing such an accurate characterization (21). This approach is the combination of

two methods: the Biomembrane Force Probe that allows probing single molecular bonds (22), and the Dual Pipette Essay that measures the interaction strength between two adhering live cells (23). Our approach consists in measuring the force necessary to break a contact between one sperm and an egg. To be as close as possible to physiology, the sperm is acrosome reacted, the egg has never seen another sperm before, and the experiments are done without any interference from additional sperm. For each gamete couple, sperm–egg adhesion and adhesion probability are probed at different locations of the egg membrane, and for each location a large number of force/distance curves directly provides the mechanical properties of the attachment between the gametes. The objectives of this study were to determine the adhesion phenotypes associated with the presence of CD9 and to analyze them in regard to the known properties of CD9 and to the gamete fusion ability. Finally, we propose a model where the fertilization is a direct consequence of CD9 controlled sperm–egg adhesion. The mechanical properties and molecular arrangements of the egg membrane required to drive a sperm–egg adhesion into fusion are described.

Results

Dramatic Reduction of Gamete Fusion Rate but Significant Increase of the Number of Sperm Bound to *Cd9* Null ZP-Free Eggs. ZP-free eggs in vitro binding and fertilization experiments were performed as described in *Material and Methods* section. Eggs collected from *Cd9* knockout and WT females were inseminated with WT sperm and examined 3 h after insemination. Fertilization rate (FR), index (FI), and number of sperm bound per egg were determined. In the absence of CD9, fertilization rate and index dramatically diminished [FR = $4 \pm 2.3\%$ (mean \pm SEM) and FI = 0.04 ± 0.02 (mean \pm SEM)] compared to the control (FR = $97.5 \pm 2.5\%$ and FI = 1.87 ± 0.14) ($P < 0.0001$, Fig. 1 *A* and *B*, respectively). By contrast, lack of CD9 significantly increased the number of sperm bound to the egg membrane (17.4 ± 1.8 versus 7.8 ± 1.9 for the WT eggs; $P = 0.0012$, Fig. 1 *C* and *D*).

Increase of Accessible Sperm Adhesion Sites on *Cd9* Null Eggs. Using the force measurement approach (cycles of approach–contact–separation of the gametes), the sperm–egg adhesion was probed at different locations of the egg membrane. During the contact phase (250 ms), the gametes had the opportunity to form one or several bonds traceable by measuring the resulting interaction

Author contributions: A.J., F.P., and C.G. designed research; A.J., A.Z., and C.G. performed research; A.J., A.Z., V.B.-L., E.P., J.P.W., F.P., and C.G. analyzed data; and A.J., A.Z., V.B.-L., E.P., F.P., and C.G. wrote the paper.

The authors declare no conflict of interest.

This article is a PNAS Direct Submission. N.D. is a guest editor invited by the Editorial Board.

¹To whom correspondence may be addressed. E-mail: gourier@lps.ens.fr.

This article contains supporting information online at www.pnas.org/lookup/suppl/doi:10.1073/pnas.1017400108/-DCSupplemental.

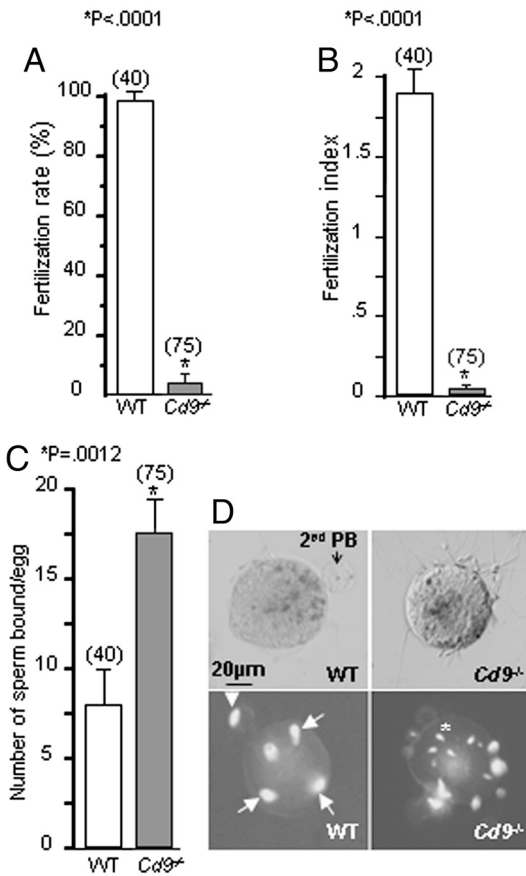


Fig. 1. Very reduced fusion rate but increased number of sperm bound on *Cd9* null eggs. In vitro fertilization and binding assays were performed at 10^5 sperm per mL during 3 h using WT (open) and *Cd9* null (gray) eggs. Data represent means (\pm S.E.M.) of three independent experiments. (A) Fertilization rate or mean (\pm S.E.M.) percentage of fertilized WT and *Cd9* null eggs. (B) Fertilization index or mean (\pm S.E.M.) of sperm number fused by egg. (C) The number of sperm that were bound to a single egg from WT and *Cd9*^{-/-} mice. (D) Sperm–egg adhesion seen in bright field (top) and sperm–egg fusion and binding observed by fluorescent microscopy (bottom) after Vectashield Dapi mounting. Decondensed sperm nucleus (arrows) are seen in the cytoplasm of the fertilized WT egg, the arrowhead indicates second polar body (PB) and asterisk represents DAPI-stained condensed sperm head, which bind to egg surface. No fused sperm are detected in the *Cd9* null egg.

force. Between 60 and 300 approach–contact–retraction cycles were performed on a contact location, and two or three locations distant from each other were probed per egg (6 *Cd9* null eggs and 6 WT eggs). This corresponds to a total of more than 2,000 contacts. On average, 46% of the contacts gave rise to adhesion for WT eggs and 75% for *Cd9* null eggs. This substantially higher adhesion probability for *Cd9* null eggs, along with higher quantity of bound sperm observed in in vitro binding experiments, demonstrates an increase of accessible sperm adhesion sites on *Cd9* null eggs.

Different Modes of Adhesion. Disappearance of One of Them on *Cd9* Null Eggs. Each approach–contact–separation cycle of the gametes gives rise to one force/distance curve. Four distinct shapes of curves, called A, B, C, and D, were obtained upon the separation phase (Fig. 2). A curves were characteristic of a contact where no bond was formed. The interaction force was zero when the gametes were fully separated. B, C, and D curves were the three kinds of curves observed when one or several links were formed between the gamete membranes. In those cases, a positive force was measured until all the formed links were broken,

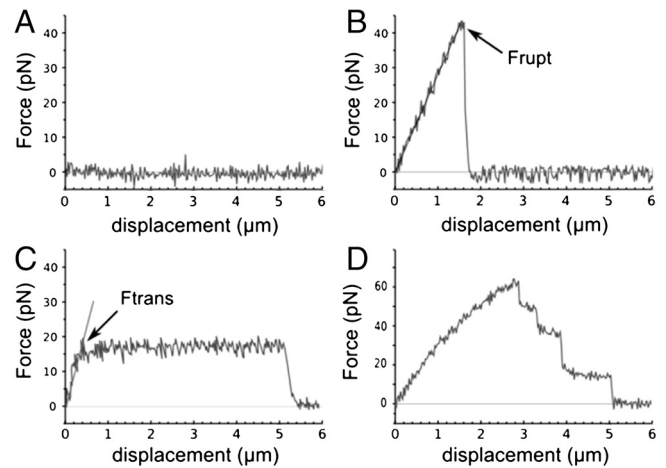


Fig. 2. Typical sperm–egg interaction force curves obtained upon gamete separation after 250 ms contact of the sperm head with the egg membrane (contact area approximately $10 \mu\text{m}^2$). On the X axis the displacement represents the deformation of the egg until effective separation of the gametes. (A) No adhesion between the two gametes, (B) adhesion with elastic deformation of the egg, (C) adhesion with extrusion of a tether from the egg membrane, (D) multiple adhesions formed in parallel in the contact area.

leading to the collapse of the force to zero. For B interaction (Fig. 2B), the linear increase of the force with the egg deformation indicates an elastic deformation of the latter until the link between the two gametes breaks at a force called “rupture force” (F_{rupt}). This force is associated to the physical separation of the two gametes. During C interaction (Fig. 2C), after an initial elastic deformation similar to B curves, an egg membrane tube was extruded from the egg (as previously reported in ref. 21) when a traction force called “transition force” (F_{trans}) was reached. In D curves, the formation in parallel of several attachment points in the contact area was revealed by a succession of jumps of forces observed in the force/distance curve. These jumps correspond to the sequential rupture of different links (24, 25). For each contact location, the rate of B, C and D curves, defined as the number of B, C or D curves normalized by the number of (B + C + D) curves, has been reported as a function of the frequency of the adhesion events (number of (B + C + D) curves divided by number of (A + B + C + D) curves) recorded at this location (Fig. 3). Fig. 3 helps determining whether each interaction shape corresponds predominantly to single or multiple attachments. Indeed, generally speaking, for two surfaces in contact bearing respectively ligands and associated receptors, the proportion of single and multiple bonds will depend on the accessible ligand and receptor densities. Single attachment will be dominant at low densities while only multiple attachments will take place at high densities (26). B curves are dominant on contact locations giving low adhesion event frequencies. Its rate decreases with increasing adhesion event frequency and vanishes at 100% adhesive events. They therefore correspond to attachments of the sperm to a single binding site on the egg. Conversely, D curves, which by definition represent sperm adhesion to multiple binding sites, see their rate increase with the adhesion event frequency. They represent about 50% of all curves at 100% adhesive frequency. The case of C curves is less straightforward. The shape of C force/distance curves (see Fig. 2C) tends to suggest a single site of adhesion because no separate jumps of force like in D curves are observed, but the increase of its rate with adhesion event frequency suggests the possibility of attachment on multiple sites. This indicates that force curves belonging to the C shape group correspond either to a single attachment site or to multiple attachment sites. There will be a majority of single attachments at low adhesion frequency and a majority of multiple binding sites at high adhesion frequency.

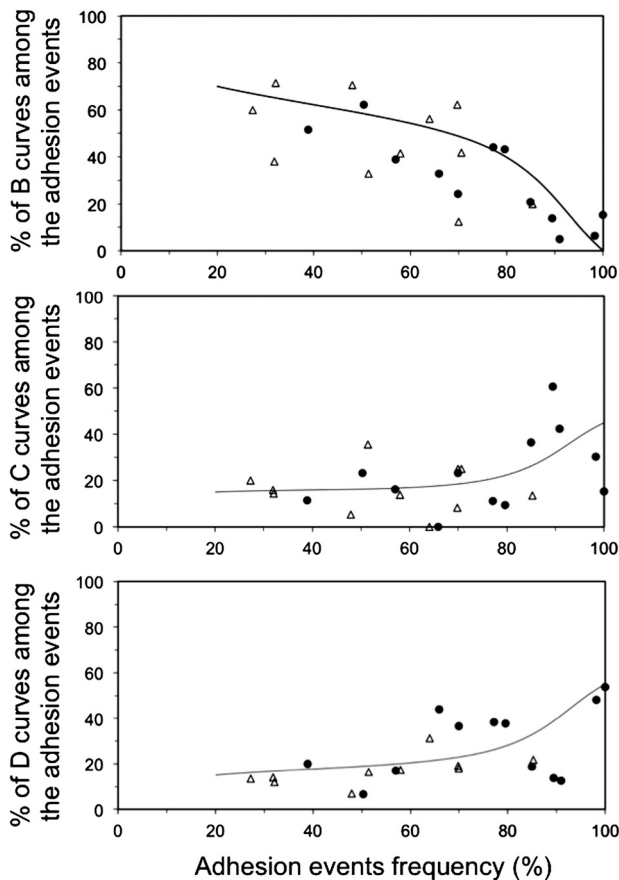


Fig. 3. Rate of the interaction curves for B, C, and D shapes as a function of the adhesion event frequency obtained at a given contact location, for WT (empty triangles) and *Cd9* null (filled circles) eggs. The lines show the variations of the curve.

To summarize, sperm–egg adhesion is due to the formation of one or several attachment points. Each of them corresponds to an elementary adhesion that belongs to one of the two following categories: (i) the adhesion that resists traction forces by deforming the cell elastically (B-shape curves), (ii) the adhesion that leads to the formation of a membrane tether under traction force (C-shape curves). For B and C single site adhesions, the histograms of F_{rupt} (for B) and F_{trans} (for C) distributions have been compared for WT and *Cd9* null eggs (Fig. 4).

For WT eggs, the distribution of F_{rupt} is bimodal with two peaks centered at 10 ± 1 (mean \pm SEM) pN and 21 ± 1 pN, while there is only one peak centered at 12 ± 1 pN for *Cd9* null eggs. The adhesive interaction associated to the second peak of the WT distribution can not be found with *Cd9* null eggs. It represents approximately 20% of the WT egg–sperm interactions. In the following, it will be called S-type adhesion (S for strong). By contrast, there is no significant difference between the *Cd9* null egg peak and the first peak of the WT distribution. They therefore most probably result from the same kind of membrane interaction, which will be called W interaction (W for weak). For C single site events, the distribution of F_{trans} is similar for WT and *Cd9* null eggs. There is one peak in each histogram centered at 14 ± 1 pN for WT and 10 ± 1 pN for *Cd9* null eggs. The interactions from which a filament is obtained will be called F interactions (F for filament). W and F interactions are shared between *Cd9* null and WT eggs while S adhesion is obtained exclusively with WT eggs.

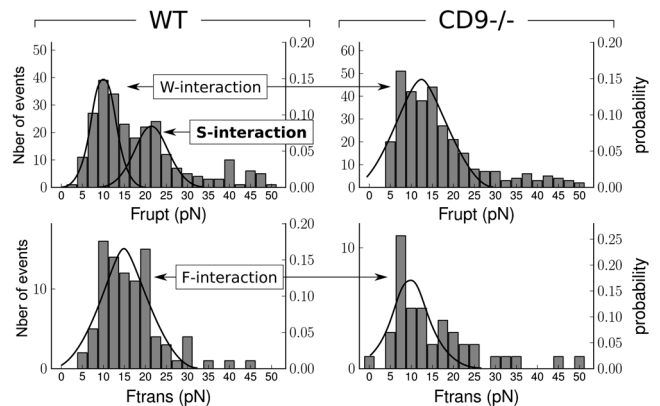


Fig. 4. Histograms of F_{rupt} and F_{trans} distribution for respectively B and C single attachments, for WT and *Cd9* null eggs. The left and right y axis respectively represent the total and normalized number of events. Top: Distribution for F_{rupt} . It is bimodal for WT eggs (W and S interactions) and monomodal (W interaction only) for *Cd9* null eggs. The adhesive interaction associated to the second peak of the WT distribution disappears without CD9. Bottom: Distribution for F_{trans} . Modomodal distribution for both WT and *Cd9* null cases.

Discussion

This study has revealed two previously unreported phenotypes correlated with the absence of CD9:

1. More sperm binding sites suggested by the increase of adhered sperm during IVF assays and confirmed by the force measurements.
2. Disappearance of the S-type interactions, as revealed by the force measurements.

These features are both related to gamete adhesion. They prove that CD9 plays a role in the prefusional adhesion stage and suggest that fusion failure may originate from an altered adhesion. These observations raise two questions: How can CD9 tetraspanins induce the changes in membrane adhesion behavior revealed by these two phenotypes? Can these changes be responsible for the drastic variation in gamete fusion ability?

Influence of CD9 on Membrane Topology and Receptor Distribution, and Consequences on Gamete Adhesion. Disappearance of S adhesion from *Cd9* null eggs means that the corresponding adhesion sites are not anymore present or accessible to sperm without CD9. By contrast, the increase in adhesion events observed on *Cd9* null eggs suggests that more adhesion sites are present or accessible to sperm on *Cd9* null egg than on WT. To elucidate the way that CD9 tetraspanin can lead to such antagonistic variation, one needs to consider the effects of *Cd9* deletion regarding (i) membrane topology, (ii) protein expression, and (iii) receptor distribution, characteristics from which membrane adhesion properties directly derive.

- Membrane topology:* WT membrane topology is significantly different from *Cd9* null eggs. Scanning electron microscopy images showed that microvilli morphology of the latter are strongly altered compared to WT eggs: They are denser, shorter, and thicker (20).
- Protein expression:* Transmission electron microscopy images of WT eggs have shown that CD9 tetraspanins (immunogold labeled) were preferentially localized on the microvilli and not on the planar regions (20). Luminescence assays have revealed on *Cd9* null egg a dramatic collapse of the immunoglobulin EWI2 (more than 90%), which has been shown to be a primary partner of CD9 on WT eggs (27). As for EWI2, we can not exclude that *Cd9* deletion may affect other genes expression.

iii. *Protein distribution*: A key function attributed to tetraspanins is to drive membrane organization through cis-interactions of membrane proteins (16–18, 28). They are able to form a network of multimolecular complexes, the “tetraspanin web” based on the assembly of primary complexes between tetraspanins and specific partners leading to protein clusters. This function of membrane organizer was first proposed in 2001 (15). Since then, it has been observed in many cell types across species (16, 29). On egg plasma membrane, CD9 has been shown to physically associate with integrin $\alpha 6 \beta 1$ known for its adhesion properties (10, 13).

Regarding the adhesive behavior experimentally measured, the crucial difference between WT and *Cd9* null eggs comes from the S-interaction events (20% of the total adhesion events). Such interactions indicate that on WT membranes, there are around 20% of adhesion sites that resist more strongly to the extrusion of lipid tethers than others. To be formed, tethers require the presence of a lipid membrane reservoir close to the adhesion site plus the possibility of having access to it. For that, the local detachment of the membrane from the inner cytostructure is necessary in order to make it accessible to filament growth (30). Membrane receptors strongly connected to the egg cytoskeleton and/or surrounded by proteins strongly connected to the egg cytoskeleton and/or embedded into patches of proteins collectively hooked to the cytoskeleton will therefore restrain the possibility of having filaments and increase the probability of having S adhesions.

In the light of these considerations, several scenarios (Fig. 5) based on the known characteristics of *Cd9* null and WT membrane (topology, protein expression, and distribution) can be considered to account for both adhesion phenotypes revealed by this study.

The simplest scenario (Fig. 5B) to explain the phenotypes observed with the BFP emerges when considering the membrane organizer function often attributed to tetraspanins in many cell types including mammalian eggs (16–18, 28). This scenario does not require different receptor composition and level of expression which is assumed to be equal to N both for WT and *Cd9* null membranes. It is only based on a receptor distribution change between WT and *Cd9* null egg membrane through CD9 induced assembling of part of these N receptors into multiprotein patches connecting together i receptors on average in the case of WT eggs (Fig. 5A). The result of such a membrane receptor reshaping is (i) the presence on WT eggs of sperm adhesion sites (i.e., the CD9 induced patches of receptors connected together, which are necessarily absent from *Cd9* null membranes), and (ii) a reduction in WT case of the effective number of binding sites since one cluster made of i connected receptors behaves like one binding site only. By contrast to an isolated receptor, which is individually anchored to the cytoskeleton, a receptor involved in a patch beneficiaries, in addition to its own anchorage, of the attachment to the cytoskeleton of all the proteins it is connected with. A sperm-egg adhesion occurring through a receptor involved into a patch will therefore provide less opportunity to form a filament than if the receptor is isolated at the membrane. The isolated receptors present on *Cd9* null and WT eggs would produce the W and F interactions, while the S adhesion observed with WT eggs would be due to CD9 induced clusters. Within the framework of this scenario, the force measurement data suggest that around 70% of the N receptors would be involved in clusters composed of $i \sim 5$ receptors (see *SI Text*).

An alternate scenario can be envisioned when considering the alteration of microvilli by CD9. Because microvilli are the primary contact of the fertilizing sperm with the egg plasma membrane, the effective sperm-egg contact area and therefore the number of binding sites accessible to the sperm depend on microvillar topology. Assuming that the same N receptors are present

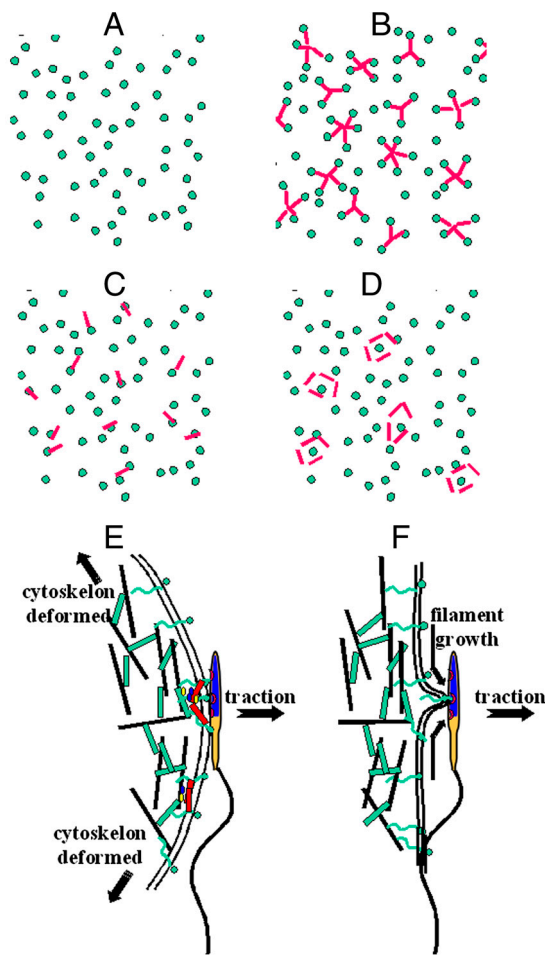


Fig. 5. Model of the involvement of CD9 in gamete adhesion and fusion processes. (A) Schematic representation (from top view) of receptor distribution (green dot) on *Cd9* null egg microvilli. (B–D) Different possible receptor and CD9 (red rod) distributions that can account for S adhesion at WT membrane (B) CD9 induces clustering of sperm receptors, (C) CD9 associates with a sperm receptor, (D) CD9 are surrounding the sperm receptor. (E) On S adhesion sites, upon traction, sperm head remains stuck to the egg membrane as long as the sperm-egg bond resists. Cytoskeleton gets deformed. Fusion process may occur. (F) Sperm-egg contact takes place on an isolated receptor. Upon traction, as soon as the receptor detaches from the cytoskeleton, a filament starts growing. The surface of contact between the gamete membranes is reduced to 1 point. Membrane fusion is impossible.

on WT and *Cd9* null egg membranes and isotropically distributed (Fig. 5A), one may expect from *Cd9* null eggs, where microvilli are shorter, thicker, and denser than on WT eggs (20), a higher accessibility of the receptors to the sperm ligands. This could explain the higher rate of W and F adhesive events observed on *Cd9* null eggs but not the loss of S adhesions. To account for the latter, one can be tempted to identify CD9 as the receptor responsible for them. However, tetraspanins are hardly ever described as receptors. Even if CD9 has been identified as a receptor for PSG17 in macrophages (31), suggesting that it may act in *trans* interaction inducing cell/cell adhesion, no membrane ligand of CD9 has ever been identified on sperm (32). As previously mentioned, EW12 immunoglobulins, also present on WT eggs, are a primary partner of CD9. In somatic cells, EW12 has been shown to directly bind to ERM (ezrin-radixin-moesin) proteins, which in turn bind to the actin filaments in the microvillar core (33). Assuming that the same occurs on eggs (ERM proteins have been shown to be also expressed on mouse eggs) (34), it can alternatively be proposed that on egg plasma membrane, a CD9 may associate with a membrane receptor (Fig. 5C). It is for

instance the case with $\alpha 6 \beta 1$ integrin (10, 13). Any sperm–egg attachment involving a receptor associated to CD9 would indirectly be anchored to the cytoskeleton through CD9-EW12-ERM-actin coupling and thus would be susceptible to produce S interaction. In fact, the sperm receptor does not even need to be directly associated to CD9 to give rise to S adhesion if it is closely surrounded by several CD9 tetraspanins strongly connected to the cytoskeleton, isolating it from the lipid reservoir that would allow extruding a filament (Fig. 5D).

The scenarios above present simple models. The reality will probably be more complicated, for instance by combining CD9 induced clusters and hiding of receptors by the longer microvilli in WT eggs. Alteration of other proteins in *CD9* null eggs cannot be excluded either. Even though the actual model cannot be determined, the phenotypes observed with the force measurement technique and the physiological conclusions that can be drawn remain the same.

S Adhesions Allow the Tight Sperm–Egg Contact Necessary to Induce Fusion. Force experiments revealed that only S-type interaction distinguishes sperm–*Cd9* null egg from sperm–WT egg adhesive behavior. IVF assays showed that *Cd9* null fertilization rate and index are negligible compared to WT eggs. Put together, these results indicate that the W and F interaction events shared by both type of eggs are not able to induce fusion. By contrast, they suggest that CD9 dependent S-type adhesions are correlated with gamete fusion. Membrane adhesion results from intermolecular bonds that connect the two membranes. It is a prerequisite for any fusion process. However, to be profusional (i.e., to be able to lead to fusion) the adhesion needs to meet several requirements, among which the most basic is to maintain the membranes in tight contact for a sufficiently long time in order to set up the molecular and membrane events involved in the fusion mechanism. Among the adhesion events observed between gametes, only S-type adhesions are susceptible to induce fusion.

Reasons for W- and F-type inefficiency and for S-type profusional abilities can be found in the analysis of the force–distance curves and histograms associated to each type of interaction. In physiology, sperm tail movement acts as a driving force for inducing sperm–egg contact but also for moving them apart once in contact, either by filament extrusion or by complete rupture of the sperm–egg adhesion. When S-type interaction occurs, the sperm head remains in tight contact with the egg membrane as long as the sperm–egg bond persists (Fig. 5E). This is also the case for W-type adhesion except that the force necessary to break the sperm–egg bond is smaller here than for S-type adhesion. The probability for the sperm flagellum to produce a force strong enough to separate the two gametes will therefore be higher for W interaction than for S adhesion, and the membrane contact time will be shorter. When F-type interaction occurs, the sperm–egg contact area is reduced to one point as soon as a filament is extruded from the egg membrane (Fig. 5F). This means that the gamete remains physically connected because of the egg membrane filament, but the sperm head is no longer laying flat on the egg membrane, contrary to S adhesion. The absence of a real contact area in an F-type interaction and the short contact time of the gamete during W adhesion are major handicaps for gamete fusion. The fact that with *Cd9* null egg, gamete adhesion results from these two nonprofusional interactions only is therefore in perfect agreement with the observed scarcity of the fusion events. By contrast, the tight contact imposed by S adhesion in addition to its robustness provide this interaction with abilities essential to allow subsequent fusion.

CD9 Generates Fusion Competent Adhesion Sites on Eggs. From the previous discussion, we propose a model in which sperm–egg fusion is a direct consequence of CD9 controlled adhesion properties. In this model, CD9 generates adhesion sites that are more

strongly anchored to the microvilli actin core than isolated receptors. The latter, present on both WT and *Cd9* null eggs, generates gamete adhesion characterized by the observed W and F interactions, which cannot induce fusion. By contrast, the adhesion sites due to CD9 give rise to S-type adhesion that imposes, during the whole interaction lifetime, a tight proximity of the gamete membranes, which is a requirement for fusion to take place. These CD9-induced adhesion sites would therefore be the actual locations where fusion is initiated.

Conclusion

Due to its capacity to detect and quantify subtle and significant local changes in membrane adhesion, the original force measurement technique used in this study can reveal, discriminate, and characterize the different types of adhesive interactions between sperm and egg plasma membrane during the fertilization process. The presence of CD9 was proven to be accompanied by the existence of a mode of strong adhesive interaction. By contrast to the weaker modes of adhesion observed for both WT and *Cd9* null eggs, the former imposes tight and long enough lasting contacts that are required for fertilization. This study proves that CD9 plays a role already in the prefusional adhesion stage of fertilization. Moreover, it strongly suggests that fusion failure may originate from an altered adhesion. We propose a model that reconciles both CD9-dependent adhesion and fusion phenotypes (no S adhesion and dramatic decrease of fusion in the absence of CD9) where sperm–egg fusion is a direct consequence of CD9 controlled sperm–egg adhesion properties.

To go further into the understanding of the fertilizing process, one could imagine investigating the nature of receptor anchoring to the cytoskeleton as well as its involvement in the establishment of fusion. This could be achieved by combining the approach presented here and drugs, antibody, or genetic strategies modifying the binding between the cell membrane and its cytoskeleton. Beyond gamete interaction, this accurate force measurement approach could be very efficient for studying other cell–cell processes where single transient molecular contacts are essential.

Material and Methods

Sperm Preparation. Sperm from 8–10 weeks old male mice were expelled from cauda epididymis and vas deferens into a 300 μ L drop of Ferticult medium containing 3% BSA under mineral oil, resulting in a concentration of approximately 10^7 sperm/mL. Sperm were then incubated at 37°C, 5% CO₂ in air for 90 min to induce capacitation. Before force measurement experiments, sperm was incubated for half an hour in a 10 μ M solution of ionophore A23187 to favor acrosomal reaction. After this treatment, less than 2% of the hyperactive sperm remained acrosome intact (see *SI Text* and Fig. S1).

Wild-Type and *Cd9* Null Eggs Preparation. Six- to eight-week-old WT and *Cd9* null female mice were superovulated by intraperitoneal injections, first of 5 IU PMSG, followed by 5 IU hCG 48 h apart. Cumulus-intact eggs were collected into a Ferticult medium drop 14 h later by tearing the oviductal ampulla from sacrificed mice. Eggs were separated from their cumulus by a brief incubation at 37°C, in presence of hyaluronidase (15 mg/mL). Mature eggs were selected on the basis of the presence of the first polar body. The zona pellucida (ZP) was subsequently removed by rapid treatment (<30 sec.) of the eggs with acidic Tyrode's solution. Eggs were then incubated for 3 h at 37°C, 5% CO₂ in air to recover from the treatment.

Zona-Free in Vitro Binding and Fertilization Assays. ZP-free eggs were inseminated with capacitated sperm for 3 h in a 50 μ L drop of medium at a final concentration of 10^5 /mL, washed and mounted in Vectashield/DAPI for observation under UV light (Zeiss Axioskop 20X microscope). The following parameters were eval-

uated: the fertilization rate (FR: the percentage of eggs fused with at least one sperm), the fertilization index (FI: the total number of fused sperm/total number of eggs), and the mean number of sperm bound to the egg. Bound sperm were counted at the egg equator in a single plane of focus by using phase optics at a magnification of 20X. Statistical analysis was performed using Statview® package. Means were compared by nonpaired *t* test. Differences were considered significant at $P < 0.05$.

Gamete Interaction Force Measurements. To probe gamete adhesion we determined the force necessary to separate a sperm in contact with an egg by measuring the deformation of a spring of controlled stiffness attached to the sperm. The spring was a biotinylated red blood cell (RBC) with a streptavidin glass bead (diameter: 3.5 μm) bound to it. The RBC stiffness $k = 125 \text{ pN}/\mu\text{m}$ was controlled by the aspiration inside the pipette that main-

tained it. The deformation Δx of the spring was obtained by tracking the position of the bead. The head of an hyperactive acrosome reacted sperm was placed in contact with the bead on which it adhered spontaneously. This RBC/bead/sperm assembly faced the egg, which was gently maintained by micropipette suction. The experimental procedure consisted of series of controlled approach–contact–retraction cycles of the egg on the spermatozoon while constantly recording the elastic deformation Δx of the spring/RBC (Fig. S2) and therefore the sperm–egg interaction force $F = k\Delta x$. The detailed parameters and the procedure of force measurement experiments are provided in *SI Text* and Figs. S2 and S3.

ACKNOWLEDGMENTS. We thank Dr. Claude Boucheix for fruitful discussions. This work was supported by the ANR-09-PIRI-0011 grant. V.B.L. was supported by a fellowship from the Pierre Gilles de Gennes foundation.

1. Coonrod SA, et al. (1999) Treatment of mouse oocytes with PI-PLC releases 70-kDa (pl 5) and 35- to 45-kDa (pl 5.5) protein clusters from the egg surface and inhibits sperm-oolemma binding and fusion. *Dev Biol* 207:334–349.
2. Alfieri JA, et al. (2003) Infertility in female mice with an oocyte-specific knockout of GPI-anchored proteins. *J Cell Sci* 116:2149–2155.
3. Rubinstein E, Ziyat A, Wolf JP, Le Naour F, Boucheix C (2006) The molecular players of sperm-egg fusion in mammals. *Semin Cell Dev Biol* 17:254–263.
4. Vjugina U, Evans JP (2008) New insights into the molecular basis of mammalian sperm-egg membrane interactions. *Front Biosci* 13:462–476.
5. Inoue N, Ikawa M, Okabe M (2010) The mechanism of sperm-egg interaction and the involvement of IZUMO1 in fusion. *Asian J Androl* 13:81–87.
6. Chen MS, et al. (1999) Role of the integrin-associated protein CD9 in binding between sperm ADAM 2 and the egg integrin $\alpha 6\beta 1$: Implications for murine fertilization. *Proc Natl Acad Sci USA* 96:11830–11835.
7. Kaji K, et al. (2000) The gamete fusion process is defective in eggs of Cd9-deficient mice. *Nat Genet* 24:279–282.
8. Le Naour F, Rubinstein E, Jasmin C, Prenant M, Boucheix C (2000) Severely reduced female fertility in CD9-deficient mice. *Science* 287:319–321.
9. Miller BJ, Georges-Labouesse E, Primakoff P, Myles DG (2000) Normal fertilization occurs with eggs lacking the integrin $\alpha 6\beta 1$ and is CD9-dependent. *J Cell Biol* 149:1289–1296.
10. Miyado K, et al. (2000) Requirement of CD9 on the egg plasma membrane for fertilization. *Science* 287:321–324.
11. Li YH, et al. (2004) Localization of CD9 in pig oocytes and its effects on sperm-egg interaction. *Reproduction* 127:151–157.
12. Zhou GB, et al. (2009) Tetraspanin CD9 in bovine oocytes and its role in fertilization. *J Reprod Dev* 55:305–308.
13. Ziyat A, et al. (2006) CD9 controls the formation of clusters that contain tetraspanins and the integrin $\{\alpha\}6\{\beta\}1$, which are involved in human and mouse gamete fusion. *J Cell Sci* 119:416–424.
14. Berditchevski F (2001) Complexes of tetraspanins with integrins: More than meets the eye. *J Cell Sci* 114:4143–4151.
15. Boucheix C, Rubinstein E (2001) Tetraspanins. *Cell Mol Life Sci* 58:1189–1205.
16. Charrin S, et al. (2009) Lateral organization of membrane proteins: Tetraspanins spin their web. *Biochem J* 420:133–154.
17. Hemler ME (2005) Tetraspanin functions and associated microdomains. *Nat Rev Mol Cell Biol* 6:801–811.
18. Levy S, Shoham T (2005) Protein–protein interactions in the tetraspanin web. *Physiol-ogy* 20:218–224.
19. Yanez-Mo M, Barreiro O, Gordon-Alonso M, Sala-Valdes M, Sanchez-Madrid F (2009) Tetraspanin-enriched microdomains: A functional unit in cell plasma membranes. *Trends Cell Biol* 19:434–446.
20. Runge KE, et al. (2007) Oocyte CD9 is enriched on the microvillar membrane and required for normal microvillar shape and distribution. *Dev Biol* 304:317–325.
21. Jegou A, et al. (2008) Mapping mouse gamete interaction forces reveal several oocyte membrane regions with different mechanical and adhesive properties. *Langmuir* 24:1451–1458.
22. Evans E, Ritchie K, Merkel R (1995) Sensitive force technique to probe molecular adhesion and structural linkages at biological interfaces. *Biophys J* 68:2580–2587.
23. Chu YS, et al. (2004) Force measurements in E-cadherin-mediated cell doublets reveal rapid adhesion strengthened by actin cytoskeleton remodeling through Rac and Cdc42. *J Cell Biol* 167:1183–1194.
24. Sun M, et al. (2005) Multiple membrane tethers probed by atomic force microscopy. *Biophys J* 89:4320–4329.
25. Girdhar G, Chen Y, Shao JY (2007) Double-tether extraction from human umbilical vein and dermal microvascular endothelial cells. *Biophys J* 92:1035–1045.
26. Zhu C, Long M, Chesla SE, Bongrand P (2002) Measuring receptor/ligand interaction at the single-bond level: Experimental and interpretative issues. *Ann Biomed Eng* 30:305–314.
27. He ZY, Gupta S, Myles D, Primakoff P (2009) Loss of surface EWI-2 on CD9 null oocytes. *Mol Reprod Dev* 76:629–636.
28. Rubinstein E, et al. (1996) CD9, CD63, CD81, and CD82 are components of a surface tetraspanin network connected to HLA-DR and VLA integrins. *Eur J Immunol* 26:2657–2665.
29. Zhu GZ, et al. (2002) Residues SFQ (173–175) in the large extracellular loop of CD9 are required for gamete fusion. *Development* 129:1995–2002.
30. Evans E, Heinrich V, Leung A, Kinoshita K (2005) Nano- to microscale dynamics of P-selectin detachment from leukocyte interfaces. I. Membrane separation from the cytoskeleton. *Biophys J* 88:2288–2298.
31. Waterhouse R, Ha C, Dveksler GS (2002) Murine CD9 is the receptor for pregnancy-specific glycoprotein 17. *J Exp Med* 195:277–282.
32. Ellerman DA, Ha C, Primakoff P, Myles DG, Dveksler GS (2003) Direct binding of the ligand PSG17 to CD9 requires a CD9 site essential for sperm-egg fusion. *Mol Biol Cell* 14:5098–5103.
33. Sala-Valdes M, et al. (2006) EWI-2 and EWI-F link the tetraspanin web to the actin cytoskeleton through their direct association with ezrin-radixin-moesin proteins. *J Biol Chem* 281:19665–19675.
34. Larson SM, et al. (2010) Cortical mechanics and meiosis II completion in mammalian oocytes are mediated by myosin-II and Ezrin-Radixin-Moesin (ERM) proteins. *Mol Biol Cell* 21:3182–3192.